ELSEVIER

Journal of Molecular Structure: THEOCHEM 770 (2006) 149–156

THEO CHEM

www.elsevier.com/locate/theochem

Kinetic study of the reaction $H_2O_2 + H \rightarrow H_2O + OH$ by ab initio and density functional theory calculations

H. Koussa, M. Bahri *, N. Jaïdane, Z. Ben Lakhdar

Laboratoire de Spectroscopie Atomique Moléculaire et Applications, Département de Physique, Faculté des Sciences, Université Tunis-El Manar, le Belvédère 1060 Tunis, Tunisie

Received 15 February 2006; received in revised form 4 May 2006; accepted 29 May 2006
Available online 6 June 2006

Abstract

Theoretical investigations on the kinetics of the elementary reaction $H_2O_2 + H \rightarrow H_2O + OH$ were performed using the transition state theory (TST). Ab initio (MP2//CASSCF) and density functional theory (B3LYP) methods were used with large basis set to predict the kinetic parameters; the classical barrier height and the pre-exponential factor. The ZPE and BSSE corrected value of the classical barrier height was predicted to be 4.1 kcal mol^{-1} for MP2//CASSCF and 4.3 kcal mol^{-1} for B3LYP calculations. The experimental value fitted from Arrhenius expressions ranges from 3.6 to 3.9 kcal mol^{-1}. Thermal rate constants of the title reaction, based on the ab initio and DFT calculations, was evaluated for temperature ranging from 200 to 2500 K assuming a direct reaction mechanism. The modeled ab initio-TST and DFT–TST rate constants calculated without tunneling were found to be in reasonable agreement with the observed ones indicating that the contribution of the tunneling effect to the reaction was predicted to be unimportant at ambient temperature.

Keywords: Hydrogen peroxide; Hydrogen atom; Ab initio; DFT; TST

1. Introduction

Hydrogen peroxide H_2O_2 is certainly an important molecule for atmospheric and biological studies. It plays a significant role in the HO_x catalytic cycle responsible for the ozone depletion in the upper atmosphere [1]. A number of forms of biological damage have been shown to be caused by H_2O_2. One several sites at which damage has been clearly shown to be due to H_2O_2 is the lens of the eye in organ culture [2]. DNA is damaged by H_2O_2 in the presence of metals [3–6]. It also causes cell death in fibroblasts [7] and bacteria [8].

During the last years, interactions involving H_2O_2 molecule in both the gas and the aqueous phase have become the focus of great attention [9–17].

Hydrogen peroxide H_2O_2 molecule, while interacting with other chemical species, can form stable complexes or react according to one of two paths: the hydrogen abstraction and the O–O bond destruction ones.

Recently, a theoretical study based on the transition state theory (TST) was carried out by some of the present authors on the reaction of the H_2O_2 molecule with H and O atoms and OH radical [17–19] according to the hydrogen abstraction path.

To our knowledge there is no theoretical kinetic study of the H_2O_2 reaction with hydrogen atom via the O–O bond destruction path leading to the H_2O molecule and OH radical.

$$H_2O_2 + H \rightarrow H_2O + OH \quad (1)$$

There have been numerous experimental measurements of the rate constant $k(T)$ of reactions (1) over a wide range of temperatures T [20].

In this work, we have used ab initio-TST and DFT–TST calculations to evaluate the rate constants $k(T)$ for reaction (1) over the range of temperature $200 \leq T \leq 2500$ K.

In the first part, we performed ab initio and DFT calculations of the electronic structures of reactants, products and activated complex involved in reaction (1). As it is well established that pre-reactive complexes, if exist, affect the reaction rates [21–24], we have searched for by calculating the minimum energy path (MEP) using the intrinsic reaction coordinates (IRC) method.

In the second part, we used the electronic structure results with the transition state theory to evaluate the rate constant $k_{TST}(T)$. Tunneling contribution to the reaction was evaluated

* Corresponding author.
E-mail address: mohamed.bahri@fss.rnu.tn (M. Bahri).

0166-1280/$ - see front matter © 2006 Elsevier B.V. All rights reserved.
doi:10.1016/j.theochem.2006.05.050

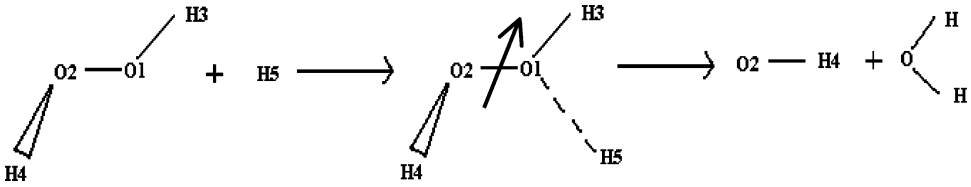

Fig. 1. Assumed mechanism for H_2O_2+H reaction.

with two methods: the Wigner [25] and the zero curvature tunneling ZCT [26] methods.

To test the reliability of the theoretical ab initio-TST and DFT–TST methods, we compared our results of $k(T)$ to the experimental ones measured by Tsang and Hampson [20] for $300 \leq T \leq 2500$ K.

2. Computational method

2.1. Electronic structure calculation

All the ab initio and DFT calculations reported in this paper were performed with the GAMESS program [27] using the aug-cc-pVTZ basis set of Dunning [28]. The reaction is considered to take place via the destruction of the O–O bond in H_2O_2 and the formation of O–H bond in H_2O as indicated in Fig. 1. Each species is taken in the ground state. The structures of the various stationary points were fully optimized without symmetry restriction and using a gradient convergence tolerance of less than 10^{-4}. The optimization algorithm used is the one based on the quadratic approximation (QA) method [29–32]. The BSSE correction (ΔBSSE) for the activated complex H_3O_2 was estimated using the Boys-Bernardi counterpoise procedure [33]

$$\Delta\mathrm{BSSE} = [E^{\mathrm{H_2O_2}}(\mathrm{H_2O_2}) - E^{\mathrm{H_3O_2}}(\mathrm{H_2O_2})] + [E^{\mathrm{H}}(\mathrm{H}) - E^{\mathrm{H_3O_2}}(\mathrm{H})] \quad (2)$$

where the upper index refers to the basis set. The geometry of H_2O_2 used in Eq. (2) is the one at the TS structure.

2.1.1. Ab initio calculation

The stationary structures, harmonic vibrational frequencies and zero point energy (ZPE) corrections for reactants, products and transition state H_3O_2 complex are determined at the CASSCF level of calculation. For the closed shell systems (H_2O_2 and H_2O) the active space contains all the bonding σ(σ_{O-O} and/or the two σ_{O-H}) and the corresponding anti-bonding σ^* orbitals. For the open shell molecular systems (H_3O_2 and OH) the active space contains, in addition to all the bonding and the anti-bonding orbitals, the orbital of the unpaired electron of the oxygen atom in OH and of the hydrogen atom in H_3O_2 complex. Using the CASSCF wave function at the optimum geometry of each species, the energy was corrected for the remaining electron correlation in a second order perturbation MP2 calculation with the MCQDPT2 method of Nakano [34,35]. All inactive electrons (not correlated at the CASSCF calculation) were included in the MP2 calculation (Fig. 2).

2.1.2. DFT calculation

All the DFT calculations relative to the reactants, the products and the transition state were performed using the B3LYP method. It includes the HF and the Becke's non-local (B88) [36] exchange and the LYP88 and VWN5 correlation functional provided, respectively, by Lee et al. [37,38] Vosko et al. [39]. For the open shell molecular systems (H_3O_2 and OH) involved in the reaction the RO-B3LYP method was used. This means that B3LYP calculation was based on the ROHF wave function of the doublet state.

2.2. IRC calculation

Starting from the CASSCF transition state geometry and Hessian matrix, we have performed the IRC calculation of the MEP for reaction (1) using the Gonzalez–Schlegel second order (GS2) method [40]. The total number of calculated points on the MEP is 95:41 points in the entrance canal and 54 points in the exit one. The MEP calculation was considered to be converged when a stationary point is reached using a gradient tolerance less than 10^{-5}.

2.3. Rate constant calculation

Rate constants are calculated, as a function of temperature T, in the zero order semi-classical interpolated transition state theory [41] assuming a direct reaction mechanism, which not involves the formation of a pre-reactive complex in the entrance canal of reaction (1). The availability of this assumption was tested in the IRC part of calculation.

In this model, information needed is only available at the reactant (R), the saddle point (≠) and the product (P) and the rate constant is given by

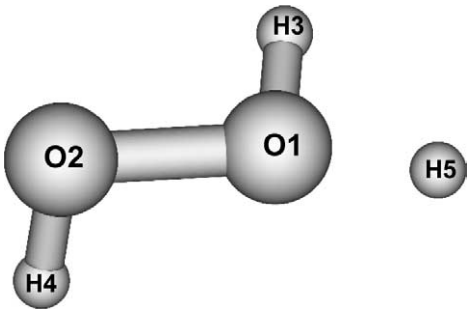

Fig. 2. Geometry of the transition state.

$$k(T) = \kappa(T) \times k_{TST}(T), \quad (3)$$

where

$$k_{TST}(T) = \frac{\sigma}{\beta h} \times \frac{Q^{\neq}(T)}{Q^{R}(T)} \times e^{-\beta V^{\neq}} \quad (4)$$

is the conventional transition state theory (TST) rate constant without tunneling correction. σ (equal 2 for this reaction) is the symmetry factor accounting for the possibility of more than one symmetry-related reaction path. $\beta = 1/K_B T$, K_B is Boltzmann's constant, h is Plank's constant, $Q^{R}(T)$ and $Q^{\neq}(T)$ are, respectively, the reactant and the transition state partition functions per unit of volume and $V^{\neq}$ is the classical barrier height. To evaluate $Q^{R}(T)$, $Q^{\neq}(T)$ and $V^{\neq}$, we need the geometry, the energy and the vibrational frequencies of reactants and activated complex. These quantities are provided by the ab initio and DFT part of calculation.

$\kappa(T)$ is a ground state transmission coefficient, which primarily accounts for tunneling correction. In this work, we have evaluated this coefficient with two different methods; the Wigner (W) [25] and the zero curvature tunneling (ZCT) [26] methods. The Wigner transmission coefficient is given by the formula

$$\kappa(T) = 1 + \frac{1}{24} \times \left| \frac{\hbar \omega^{\neq}}{K_B T} \right|^2 \quad (5)$$

$\omega^{\neq}$ is the imaginary frequency of the transition state.

For details about the ZCT model, see indicated reference. The two tunneling corrected rate constants are noted, respectively, by $k_{TST/W}$ and $k_{TST/ZCT}$.

All the rate constant calculations were done with the POLYRATE 8.0 program [42].

3. Resuls and discussion

3.1. Electronic structure calculations

In this section, we present our results of the ab initio and DFT part of calculation relative to the minimum energy structure, the harmonic vibrational frequencies and the energy of each species implied in reaction (1). As rotational and vibrational partition functions of reactants and the activated complex which serve to evaluate the TST rate constant depend, respectively, on the optimized structures and the vibrational frequencies we test the reliability of our ab initio and DFT calculations by comparing our results with the experimental ones.

3.1.1. Minimum energy structure

The calculated CASSCF and RO-B3LYP geometrical parameters for the stationary structure of OH, H_2O and H_2O_2 and the activated complex H_3O_2 are given and compared to available experimental ones in Table 1. Inspection of this table shows that for both methods calculated parameters of reactants and products agree well with the experimental ones. The disagreement do not exceeds 1% for bond lengths and 4% for angles. This agreement between calculated and experimental structures support our calculations and indicates that the resulting moments of inertia of H_2O_2 molecule, which are useful in calculating rotational partition function, are predicted with a reasonable accuracy.

Table 1
Calculated geometrical parameters of OH, H_2O, H_2O_2 and H_3O_2 (bond lengths in angstrom, angles in degrees)

System	Parameters[a]	CASSCF	RO-B3LYP	Exp.[b]
OH	R(O–H)	0.974	0.975	0.969
H_2O	R(O–H)	0.962	0.961	0.958
	θ(HOH)	103.5	105.1	104.5
H_2O_2	R(O–O)	1.474	1.451	1.464
	R(O–H)	0.967	0.967	0.965
	θ(OOH)	99.26	100.7	99.4
	α(HOOH)	115.92	113.5	111.8
H_3O_2[c]	R(O1–O2)	1.668	1.526	
	R(O1–H3)	0.976	0.968	
	R(O2–H4)	0.969	0.967	
	R(O1–H5)	1.592	1.628	
	θ(O2O1H3)	93.6	99.1	
	θ(O1O2H4)	94.4	98.9	
	θ(H5O1O2)	175.2	164.3	
	α(H4O2O1H3)	133.1	117.9	
	α(H5O1H3O2)	179.2	174.3	

[a] R, stretch; θ, bending angle; α, tortional angle.
[b] Ref [43] for OH and H_2O_2 and Ref [44] for H_2O.
[c] See Fig. 2.

The predicted structure of the activated complex indicates that in order for reaction (1) to take place via O–O bond destruction path, the later bond must be stretched by about 13% for CASSCF and 5% for RO-B3LYP calculations. The OH

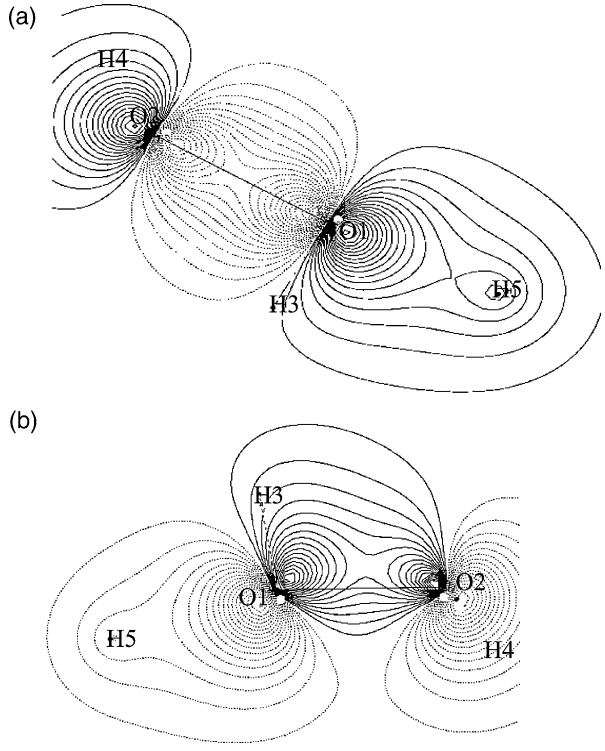

Fig. 3. Isodensity curves corresponding to the σ(O1–O2) orbital in H_2O_2: (a) ab initio and (b) DFT.

bond thus formed at the TS is greater than its homologous in the product H_2O by about 65.5% for CASSCF and 69.4% for RO-B3LYP methods. Both methods provide a reactant-like character for the transition state, which is consistent with the exothermic character of the reaction. The predicted values of the (H5O1O2) bending angles and the (H5O1H3O2) dihedral one are, respectively, 175.2 and 179.2° for CASSCF and 164.3 and 174.4° for RO-B3LYP methods. This means that, for both methods, the preferred bringing together of H_2O_2 molecule and H atom for reaction according to the indicated path is the one where H5, O1, O2 atoms are nearly collinear and H5 lies in the (O1O2H3) plane. Fig. 3 shows the CASSCF and B3LYP isodensity curves of the σ(O1–O2) orbital in the H_3O_2 activated complex. We note that the probability to find the electrons occupying the σ(O1–O2) in the region between O1 and H5 atoms is important. So the O1–O2 and O1–H5 bonds at the TS appear ready to be, respectively, broken and formed. This is consistent with the O–O bond destruction path hypothesis and represents the first indication that we have located the adequate transition structure.

3.1.2. Vibrational frequencies

The calculated CASSCF and RO-B3LYP harmonic vibrational frequencies of OH, H_2O, H_2O_2 and H_3O_2 are listed with the available experimental ones in Table 2. We note that the disagreement between calculated and experimental frequencies of OH, H_2O and H_2O_2 for all vibrational modes never exceeds 8.1% and can go below 1.5%. This indicates that the resulting vibrational partition function of H_2O_2, which are useful in calculating rate constants, are predicted with a reasonable accuracy.

Table 2
Harmonic vibrational frequencies (cm^{-1}) of the equilibrium structure for OH, H_2O, H_2O_2 and H_3O_2

Molecular system	CASSCF	RO-B3LYP	Exp.
OH	3624(1.5)	3666(2.7)	3570[a]
H_2O	1705(6.9)	1625(1.9)	1595[b]
	3792(3.9)	3765(3.1)	3651
	3893(3.6)	3878(3.2)	3756
H_2O_2	341(8.1)	375(1.1)	371[c]
	845(3.7)	949(8.1)	878[d]
	1340(4.9)	1326(4.1)	1274[e]
	1452(4.1)	1440(3.3)	1394[f]
	3736(3.5)	3728(3.3)	3610[c]
	3740(3.6)	3741(3.4)	3619[c]
H_3O_2	238	146	
	390	332	
	449	409	
	632	828	
	1130	1246	
	1284	1357	
	3718	3736	
	3722	3746	
	1624 I	968 I	

Value in parentheses represents the error (in %) of calculations with respect to experiment.
[a] Ref. [45].
[b] Ref. [46].
[c] Ref. [47].
[d] Ref. [48].
[e] Ref. [49].
[f] Ref. [50].

Table 3
Decomposition of the imaginary normal mode into internal coordinates

Internal coordinate	CASSCF	RO-B3LYP
R(O1–O2)	0.19767	0.1834
R(O1–H3)	−0.00015	−0.0011
R(O2–H4)	−0.00009	−0.0002
R(O1–H5)	−0.93695	−0.9522
θ(O2O1H3)	−0.05761	−0.0458
θ(O1O2H4)	−0.03232	−0.0302
θ(H5O1O2)	−0.00147	−0.0137
α(H4O2O1H3)	0.00407	0.0088
α(H5O1O2H4)	0.01630	0.0190
α(H5O1H3O2)	0.00001	−0.00007

The calculated Hessian matrix of the transition state structure was found to possess only one imaginary frequency $\omega^{\neq}$, which have a magnitude of 1624 cm^{-1} for CASSCF and 968 cm^{-1} for B3LYP calculations. The imaginary normal mode is decomposed into the nine internal coordinates by Boatz and Gordon's method [51]. The contribution coefficient of each internal coordinate to this mode is given in Table 3. It is clear that for both methods, major contribution comes from the R(O1–O2) and R(O1–H5) bond lengths which involve the three O1, O2 and H5 reactive atoms. So the transition state eigenvector associated to this unique imaginary frequency is a motion, which corresponds, at the same time, to the destruction of the O1–O2 bond and to the formation of the O1–H5 one. This is what is exactly observed when this imaginary mode is animated using the MOLDEN package [52]. This result represents the second indication that we have located the right transition state.

3.1.3. Energetics

The calculated CASSCF, MP2//CASSCF and RO-B3LYP total energies of all species involved in reaction (1) are listed in Table 4. The total energies used to evaluate the BSSE correction according to Eq. (3) were collected in Table 5. Using the energy values of Table 4, the reaction energy E_r and the classical barrier height $V^{\neq}$ of the studied reaction were evaluated.

$$E_r = E(OH) + E(H_2O) - [E(H) + E(H_2O_2)] \quad (6)$$

$$V^{\neq} = E(H_3O_2) - [E(H) + E(H_2O_2)] \quad (7)$$

Table 4
Total energies (a.u.) of the reactants (H_2O_2, H), the products (H_2O, OH) and the activated complex (H_3O_2)

System[a]	CASSCF	MP2// CASSCF	RO-B3LYP
OH	−75.44060969(5.2)	−75.65458631	−75.73433759(5.2)
H_2O	−76.11279257(13.4)	−76.34564033	−76.43029916(13.5)
H_2O_2	−150.94329490(16.4)	−151.38830195	−151.55294368(16.5)
H_3O_2	−151.42098330(16.5)	−151.88304025	−152.04646929(16.9)

Values in parentheses are the ZPE corrections (kcal mol^{-1}).
[a] The H atom energy, calculated at the ROHF level is 0.49983384 a.u.

Table 5
Total energies (a.u) used to evaluate the BSSE correction (kcal molecule^{-1}) for the H_3O_2 complex

	MP2//CASSCF	RO-B3LYP
$E^{H3O2}(H_2O_2)$	−151.38028858	−151.55062297
$E^{H2O2}(H_2O_2)$	−151.37898582	−151.55056914
ΔBSSE[a]	0.8	0.03

($E^{H3O2}(H) = -0.499837197$ and $E^{H}(H) = -0.4998338396$ a.u. are calculated at the ROHF level).
[a] See Eq. (2).

Table 6
Reaction energy E_r and activation barrier $V^{\neq}$ (kcal molecule^{-1})

	MP2//CASSCF	RO-B3LYP	Exp.[a]
E_r	−70.3 (−68.1)	−70.2 (−68.2)	−68.2
$V^{\neq}$	3.2 (4.1)	4.0 (4.3)	3.6–4.0

Values in parenthesis are the BSSE and/or ZPE corrected ones.
[a] Ref. [20].

The resulting MP2//CASSCF and RO-B3LYP values of E_r and $V^{\neq}$ were collected with the experimental values in Table 6. Inspection of this table shows that the ZPE corrected value of E_r predicted by the two methods closes to the experimental one with an error less than 0.1 kcal mol^{-1}. Such agreement between calculated and experimental reaction energy is rarely observed since the mean error on the E_r value is about 1.5 kcal mol^{-1} for high correlated ab initio level of calculation and ranges from 3 to 4 kcal mol^{-1} for B3LYP method [53]. The calculated MP2//CASSCF value of $V^{\neq}$ is found to be 3.2 kcal mol^{-1} and is increased to 4.1 kcal mol^{-1} when BSSE and ZPE corrections are included. The later value of $V^{\neq}$ overestimates the experimental one by only 0.6 kcal mol^{-1}. So the MP2//CASSCF method predicts the barrier height of reaction (1) with a reasonable accuracy. This is expected since high correlated ab initio levels of calculation, when used with large basis set, were known to give accurate barrier heights. The unexpected result is the predicted RO-B3LYP value of $V^{\neq}$ (4.3 kcal mol^{-1}) which overestimate the ab initio and the experimental ones by, respectively, 0.2 and 0.7 kcal mol^{-1}. It is surprising since it is well established that B3LYP is one of some DFT based methods, which largely underestimate the barrier heights of reactions [53–55]. In most cases, the test made on the B3LYP method in reproducing barrier heights involves hydrogen-atom transfer reactions. So our DFT calculation on this reaction, which is not an hydrogen abstraction one, shows that B3LYP can be an effective method to use in predicting accurate reaction and activation energies for reactions occurring according to a path other than that of the hydrogen abstraction.

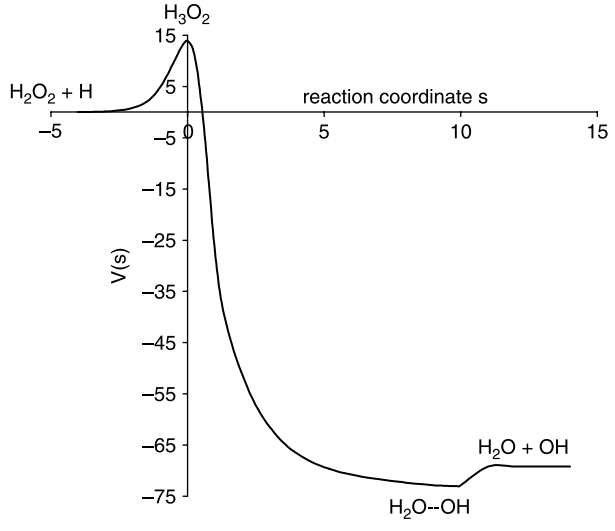

Fig. 4. CASSCF minimum energy path $v(s)$ in kcal/mol.

The MP2//CASSCF and RO-B3LYB values of E_r and $V^{\neq}$ used in the kinetic part of calculation are the BSSE and/or ZPE corrected ones.

3.2. Minimum energy path

The MEP $V(s)$ as a function of the reaction coordinate s calculated at the CASSCF level using the IRC method was shown in Fig. 4. In Table 7, we reported only 18 points among the 96 calculated ones on the MEP. Fig. 4 shows that no possible pre-reactive complex in the entrance canal of reaction (1) can be formed. This supports our rate constant calculation, which not takes into account the existence of such complex. In the exit canal, the IRC calculation converges towards an intermediate complex H_2O–OH more stable than the products by about 4 kcal mol^{-1}.

3.3. Rate constant calculation

The calculated (ab initio)-TST and DFT–TST rate constant of reaction (1) for temperatures ranging from 200 to 2500 K are listed and compared to the experimental values Exp, respectively, in Tables 8 and 9. Figs. 5 and 6 show, respectively, the

Table 7
CASSCF total energies (a.u.) of 21 points on the minimum energy path

Reaction coordinates sqrt(amu)-Bohr	Minimum energy path $V(s)$
−∞ (Reactants)	−151.44312874
−4.0	−151.44311083
−3.5	−151.44306034
−3.0	−151.44293368
−2.5	−151.44260937
−2.0	−151.44180559
−1.5	−151.43993722
−1.0	−151.43535499
−0.5	−151.42749144
0.0 (TS)	−151.42098330
1.0	−151.48629049
2.0	−151.52452871
3.0	−151.54088792
4.0	−151.54925440
5.0	−151.55356791
6.0	−151.55589516
7.0	−151.55731655
8.0	−151.55838811
9.0	−151.55917918
10.0	−151.55951716
+∞ (Products)	−151.55340226

Table 8
Calculated ab initio-TST rate constants ($cm^3\ molecule^{-1}\ s^{-1}$) compared to experimental values

T (k)	k_{TST}	$k_{TST/W}$	$k_{TST/ZCT}$	Exp[a]
200	9.72(−16)	6.50(−15)	6.70(−14)	
250	7.96(−15)	3.68(−14)	1.30(−13)	
298	3.20(−14)	1.14(−13)	2.32(−13)	
300	3.36(−14)	1.18(−13)	2.38(−13)	5.09(−14)
350	9.68(−14)	2.76(−13)	4.12(−13)	1.31(−13)
400	2.20(−13)	5.32(−13)	6.68(−13)	2.69(−13)
450	4.26(−13)	9.04(−13)	1.03(−12)	4.69(−13)
500	7.34(−13)	1.40(−12)	1.50(−12)	7.32(−13)
550	1.17(−12)	2.04(−12)	2.10(−12)	1.05(−12)
600	1.74(−12)	2.82(−12)	2.84(−12)	1.42(−12)
650	2.44(−12)	3.76(−12)	3.74(−12)	1.84(−12)
700	3.32(−12)	4.88(−12)	4.78(−12)	2.29(−12)
750	4.38(−12)	6.16(−12)	6.02(−12)	2.77(−12)
800	5.60(−12)	7.60(−12)	7.40(−12)	3.28(−12)
850	7.00(−12)	9.22(−12)	8.96(−12)	3.80(−12)
900	8.60(−12)	1.10(−11)	1.07(−11)	4.33(−12)
950	1.04(−11)	1.30(−11)	1.26(−11)	4.87(−12)
1000	1.23(−11)	1.51(−11)	1.47(−11)	5.41(−12)
1050	1.45(−11)	1.75(−11)	1.70(−11)	5.95(−12)
1100	1.68(−11)	2.00(−11)	1.95(−11)	6.49(−12)
1150	1.93(−11)	2.26(−11)	2.20(−11)	7.02(−12)
1200	2.20(−11)	2.54(−11)	2.48(−11)	7.55(−12)
1250	2.48(−11)	2.84(−11)	2.78(−11)	8.07(−12)
1300	2.78(−11)	3.16(−11)	3.10(−11)	8.58(−12)
1350	3.12(−11)	3.50(−11)	3.44(−11)	9.09(−12)
1400	3.46(−11)	3.86(−11)	3.78(−11)	9.58(−12)
1450	3.82(−11)	4.22(−11)	4.14(−11)	1.00(−11)
1500	4.18(−11)	4.62(−11)	4.54(−11)	1.05(−11)
1550	4.58(−11)	5.02(−11)	4.94(−11)	1.10(−11)
1600	5.00(−11)	5.44(−11)	5.36(−11)	1.14(−11)
1650	5.42(−11)	5.88(−11)	5.78(−11)	1.19(−11)
1700	5.86(−11)	6.32(−11)	6.24(−11)	1.23(−11)
1800	6.84(−11)	7.28(−11)	7.18(−11)	1.31(−11)
1900	7.78(−11)	8.28(−11)	8.18(−11)	1.39(−11)
2000	8.84(−11)	9.34(−11)	9.24(−11)	1.47(−11)
2100	9.96(−11)	1.05(−10)	1.04(−10)	1.54(−11)
2200	1.11(−10)	1.17(−10)	1.15(−10)	1.61(−11)
2300	1.24(−10)	1.29(−10)	1.28(−10)	1.67(−11)
2400	1.36(−10)	1.42(−10)	1.41(−10)	1.73(−11)
2500	1.50(−10)	1.55(−10)	1.54(−10)	1.79(−11)

Power of 10 in parentheses.
[a] Ref. [20].

Table 9
Calculated DFT–TST rate constants ($cm^3\ molecule^{-1}\ s^{-1}$) compared to experimental values

T (K)	k_{TST}	$k_{TST/W}$	$k_{TST/ZCT}$	Exp.
200	7.98(−16)	2.40(−15)	6.80(−15)	
250	7.56(−15)	1.73(−14)	2.78(−14)	
298	3.34(−14)	6.38(−14)	8.18(−14)	
300	3.52(−14)	6.68(−14)	8.52(−14)	5.09(−14)
350	1.09(−13)	1.82(−13)	2.06(−13)	1.31(−13)
400	2.62(−13)	3.94(−13)	4.24(−13)	2.69(−13)
450	5.28(−13)	7.40(−13)	7.72(−13)	4.69(−13)
500	9.42(−13)	1.25(−12)	1.28(−12)	7.32(−13)
550	1.54(−12)	1.95(−12)	1.97(−12)	1.05(−12)
600	2.32(−12)	2.84(−12)	2.86(−12)	1.42(−12)
650	3.34(−12)	3.98(−12)	4.00(−12)	1.84(−12)
700	4.62(−12)	5.38(−12)	5.38(−12)	2.29(−12)
750	6.14(−12)	7.02(−12)	7.02(−12)	2.77(−12)
800	7.94(−12)	8.94(−12)	8.92(−12)	3.28(−12)
850	1.00(−11)	1.11(−11)	1.11(−11)	3.8(−12)
900	1.24(−11)	1.36(−11)	1.36(−11)	4.33(−12)
950	1.50(−11)	1.64(−11)	1.63(−11)	4.87(−12)
1000	1.79(−11)	1.94(−11)	1.93(−11)	5.41(−12)
1050	2.10(−11)	2.26(−11)	2.26(−11)	5.95(−12)
1100	2.46(−11)	2.62(−11)	2.62(−11)	6.49(−12)
1150	2.84(−11)	3.02(−11)	3.00(−11)	7.02(−12)
1200	3.24(−11)	3.42(−11)	3.42(−11)	7.55(−12)
1250	3.68(−11)	3.88(−11)	3.86(−11)	8.07(−12)
1300	4.14(−11)	4.34(−11)	4.34(−11)	8.58(−12)
1350	4.64(−11)	4.84(−11)	4.84(−11)	9.09(−12)
1400	5.16(−11)	5.38(−11)	5.36(−11)	9.58(−12)
1450	5.70(−11)	5.92(−11)	5.92(−11)	1.00(−11)
1500	6.28(−11)	5.92(−11)	6.48(−11)	1.05(−11)
1550	6.88(−11)	6.50(−11)	7.10(−11)	1.10(−11)
1600	7.50(−11)	7.10(−11)	7.72(−11)	1.14(−11)
1650	8.16(−11)	8.40(−11)	8.38(−11)	1.19(−11)
1700	8.84(−11)	9.08(−11)	9.06(−11)	1.23(−11)
1800	1.03(−10)	1.05(−10)	1.10(−10)	1.31(−11)
1900	1.18(−10)	1.20(−10)	1.20(−10)	1.39(−11)
2000	1.34(−10)	1.37(−10)	1.36(−10)	1.47(−11)
2100	1.51(−10)	1.54(−10)	1.54(−10)	1.54(−11)
2200	1.69(−10)	1.72(−10)	1.72(−10)	1.61(−11)
2300	1.88(−10)	1.91(−10)	1.90(−10)	1.67(−11)
2400	2.06(−10)	2.10(−10)	2.10(−10)	1.73(−11)
2500	2.26(−10)	2.30(−10)	2.30(−10)	1.79(−11)

logarithm plot of the ab initio-TST and the DFT–TST rate constants k_{TST}, $k_{TST/W}$ and $k_{TST/ZCT}$ and the measured ones versus 1000/T (K). It is clear from these figures that TST/W and TST/ZCT methods overestimate the experimental result for all considered temperatures. At low temperatures the best agreement between the experimental and the modeled rate constants was obtained for the TST ones calculated without taking into account the tunneling effect. The experimental error on the $\log k$ values is about 0.3 [20] for all considered temperatures. Introducing this error, the values of $\log k$ range from the lower limit $Exp_{min} = \log k - 0.3$ to the upper one $Exp_{max} = \log k + 0.3$. Exp_{min} and Exp_{max} values were reported also in Figs. 5 and 6. We note that taking into account the experimental error does not affect the fact that, among the calculated rate constant, the TST values are the most accurately predicted ones. As the calculated MP2//CASSCF and

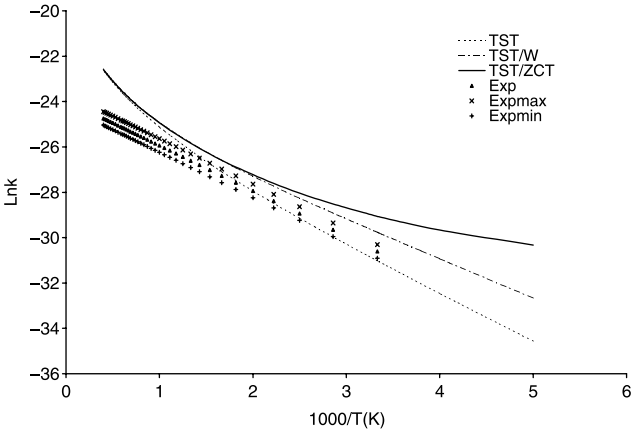

Fig. 5. Plot of logarithm of the ab initio-TST rate constant ($cm^3\ molecule^{-1}\ s^{-1}$) versus 1000/$T$ (K) compared to the experimental ones.

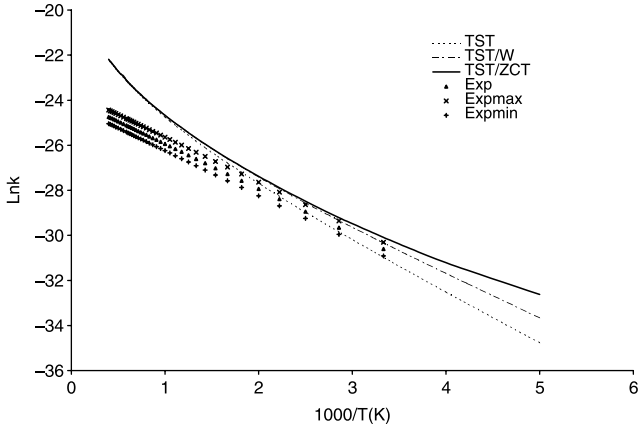

Fig. 6. Plot of logarithm of the DFT–TST rate constant (cm^3 $molecule^{-1}$ s^{-1}) versus 1000/T (K) compared to the experimental ones.

RO-B3LYP barrier height of reaction (1) agree well with the experimental value and so the resulting error on the evaluation of the rate constants is small, we can deduce that our ab initio and DFT calculations predict that tunneling contribution to reaction (1) is not important at ambient temperature. At high temperature (about 1500 K) our ab initio-TST and DFT–TST modeled k_{TST} rate constants overestimate the experimental ones by a factor (k_{TST}/k_{exp}) of about, respectively, 2 and 3. This disagreement factor increases with increasing temperature and can reach for $T=2500$ K a value of 8 for the ab initio-TST used method and a value of 12 for the DFT–TST one. This disagreement, at high temperature, between the TST rate constants and the experimental ones can be due to the anharmonicity effects (not included here) especially for the bending vibrations in the activated complex [56].

4. Conclusion

We have performed ab initio (MP2//CASSCF) and DFT (B3LYP) calculations using a basis set that is large enough to determine electronic structures of reactants, products and activated complex involved in $H_2O_2+H\rightarrow H_2O+OH$ reaction which was considered to take place via the destruction of the O–O bond in H_2O_2 and the formation of O–H one in H_2O. The BSSE or/and ZPE corrected values of the reaction energy and the classical barrier height were found to be, respectively, -68.1 and 4.1 kcal mol^{-1} for ab initio and -68.2 and 4.3 kcal mol^{-1} for DFT calculations. The experimental value of the reaction energy is about -68.2 kcal mol^{-1} and that of the barrier height lies between 3.6 and 3.9 kcal mol^{-1}. So the well-established deficiency of the B3LYP method in reproducing accurate reaction and activation energy for hydrogen abstraction reactions was not observed here. The calculated ab initio and DFT minimum energy structures and vibrational frequencies of the reactant H_2O_2 and the products (OH and H_2O) were found to be in reasonable agreement with the experimental results. The predicted structure of the activated complex H_3O_2 shows that, for reaction (1) to take place according to the indicated path, the reactive atom H must be near collinear to the oxygen atoms and lies in the OOH plane of H_2O_2. These ab initio and DFT electronic structure results were used with the transition state theory to evaluate the thermal rate constants over the range of temperature $200\leq T\leq 2500$ K assuming a direct reaction mechanism. Compared to experimental results the rate constants k_{TST} calculate without tunneling effect were found to be the most accurately predicted ones. This can be an indication that the tunneling effect contribution to the title reaction is not important at ambient temperature.

Acknowledgements

The authors are grateful to Prof. Donald G. Truhlar, Department of Chemistry University of Minnesota, for the license access to POLYRATE program.

References

[1] M. Bellini, E. Catacchini, P. De Natale, G. Di Lonardo, L. Fusina, M. Inguscio, E. Venuti, J. Mol. Spectrosc. 177 (1996) 115.
[2] J.S. Zigler Jr., H.M. Jernigan Jr., D. Garland, V.N. Reddy, Arch. Biochem. Biophys. 241 (1985) 163.
[3] Y. Uchida, H. Shigematu, K. Yamafuji, Enzymologia 6 (1965) 369.
[4] K.M. Keller, E.C. Pollard, Int. J. Radiat. Biol. 31 (1977) 407.
[5] Y. Massie, M. Kitahara, K. Maeda, H. Umezawa, Biochim. Biophys. Acta 272 (1972) 539.
[6] R. Meneghini, M.E. Hoffmann, Biochim. Biophys. Acta. 608 (1980) 167.
[7] R.H. Simon, C.H. Scoggin, D. Patterson, J. Biol. Chem. 256 (1981) 7181.
[8] J.P. McCormick, J.R. Fischer, J.P. Pachlatki, A.A. Eisenstark, Science 191 (1976) 468.
[9] Y. Shi, Z.Y. Zhou, J. Mol. Struct. 113 (2004) 674.
[10] A.M. Pimenta, S.H.F. Scafi, C. Pasquini, I.M. Raimundo Jr., J.J.R. Rohwedder, M. da C, B.S.M. Montenegro, A.N. Araujo, J. Near, Infrared Spectrosc. 11 (2003) 49.
[11] H. Voraberger, V. Ribitsch, M. Janotta, B. Mizaikoff, Appl. Spectrosc. 57 (2003) 574.
[12] S.A. Kulkarni, L.J. Bartolotti, R.K. Pathak, Chem. Phys. Lett. 372 (2003) 620.
[13] A. Engdahl, B. Nelader, Chem. Phys. 293 (2003) 203.
[14] R. Wysokinski, D. Michalska, D.C. Bienko, T. Zeegers-Huyskens, J. Phys. Chem. A. 107 (2003) 8730.
[15] W. De Jesus-Bonilla, E. Ramirez-Melendez, J. Cerda, J. Lopez-Garriga, Biospectroscopy 67 (2002) 178.
[16] D.A. Proshlyakov, T. Ogura, K. Shinzawa-Itoh, S. Yoshikawa, T. Kitagawa, Biochemistry 35 (1996) 76.
[17] Y. Tarchouna, M. Bahri, N. Jaïdane, Z. Ben Lakdar, J.P. Flament, J. Chem. Phys. 118 (2003) 1189.
[18] Y. Tarchouna, M. Bahri, N. Jaïdane, Z. Ben Lakdar, J.P. Flament, J. Mol Struct. (THEOCHEM) 664–665 (2003) 189.
[19] M. Bahri, Y. Tarchouna, N. Jaïdane, Z. Ben Lakdar, J.P. Flament, J. Mol. Struct. (THEOCHEM) 664–665 (2003) 229.
[20] D.L. Baulch, C.J. Cobos, R.A. Cox, C. Esser, P. Frank, h. Just, J.A. Kerr, M.J. Pilling, J. Troe, R.W. Walker, J. Warnatz, J. Phys. Chem. Ref. Data. 21 (1992) 506.
[21] J. Raul Alvarez-Idaboy, Nelaine Mora-Diez, Russel.J. Boyd, Annik Vivier-Bunge, J. Am. Chem. Soc. 123 (2001) 2018.
[22] Annia Galano, J. Raul Alvarez-Idaboy, Ma. Esther Ruiz-Santoyo, Annik Vivier-Bunge, J. Phys. Chem. A 106 (2002) 9520.
[23] Erin.E. Greenwald, Simon.W. North, Yuri Georgievskii, Stephen.J. Klippenstein, J. Phys. Chem. A 109 (2005) 6031.
[24] Françoise Caralp, Wendell Forst, Eric Hénon, Astrid Bergeat, Frederic Bohr, Phys. Chem. Chem. Phys. 8 (2006) 1072.
[25] E. Wigner, Z. Phys, Chem. B 19 (1932) 203.

[26] A. Gonzalez-Lafont, T.N. Truong, D.G. Truhlar, J. Chem. Phys. 95 (1991) 8875.
[27] M.W. Schmidt, K.K. Baldridge, J.A. Boatz, S.T. Elbert, M.S. Gorden, J.H. Jensen, S. Koseki, N. Matsunaga, K.A. Nguyen, S.J. Su, T.L. Windus, M. Dupuis, J.A. Montgomery, J. Comput. Chem. 14 (1993) 1347.
[28] T.H. Dunning Jr., J. Chem. Phys. 90 (1989) 1007.
[29] J. Baker, J. Comput. Chem. 7 (1986) 385.
[30] T. Helgaker, Chem. Phys. Lett. 182 (1991) 305.
[31] P. Culot, G. Dive, V.H. Nguyen, J.M. Ghuysen, Theor. Chim. Acta 82 (1992) 189.
[32] F. Jensen, J. Chem. Phys. 102 (1995) 6706.
[33] S.F. Boys, F. Bernardi, Mol. Phys. 19 (1970) 553.
[34] H. Nakano, J. Chem. Phys. 99 (1993) 7983.
[35] H. Nakano, Chem. Phys. Lett. 207 (1993) 372.
[36] A.D. Becke, Phys. Rev. A. 38 (1988) 3098.
[37] C. Lee, W. Yang, R.G. Parr, Phys. Rev. B 37 (1988) 785.
[38] B. Miehlich, A. Savin, H. Stoll, H. Preuss, Chem. Phys. Lett. 157 (1989) 200.
[39] S.H. Vosko, L. Wilk, M. Nusair, Can. J. Phys. 58 (1980) 1200.
[40] C. Gonzalez, H.B. Schlegel, J. Chem. Phys. 90 (1989) 2154.
[41] T.N. Truong, D.G. Truhlar, J. Chem. Phys. 93 (1990) 1761.
[42] R. Steckler, Y.Y. Chuang, P.L. Fast, E.L. Coitino, J.C. Corchado, W.P. Hu, Y.P. Liu, G.C. Lynch, K.A. Nguyen, C.F. Jackels, M.Z. Gu, I. Rossi, S. Clayton, V.S. Mellissas, B.C. Garrett, A.D. Issacson, D.G. Truhlar, POLYRATE-version 7.3.1, University of Minnesotta, Minneapolis, (1997).
[43] R. Fourier, A.E. De Pristo, J. Chem. Phys. 96 (1992) 1183.
[44] M.D. Harmony, V.W. Laurie, R.L. Kuczmowski, R.H. Schwendeman, D.A. Ramsay, F.J. Lovas, W.J. Lafferty, A.G. Maki, J. Phys. Chem. Ref. Data. 8 (1979) 619.
[45] M.W. Chase Jr., C.A. Davies, J.R. Downey Jr., D.J. Frurip, R.A. mc donald, A.N. Syverud (Eds.), third ed., JANAF Thermodynamical Tables, vol. 14, National Bureau of Standards, Washington, DC, 1985.
[46] T. Shimanouchi, Tables of Molecular Vibrational Frequencies Consolidated Volume I, National Bureau of Standards (1972) 1–160.
[47] W.B. Olson, R.H. Hunt, B.W. Young, A.G. Maki, J.W. Brault, J. Mol. Spectrosc. 127 (1988) 12.
[48] C. Camy-Peyret, J.M. Flaud, J.W.C. Johns, M. Noel, J. Mol. Spectrosc. 155 (1992) 84.
[49] S. Klee, M. Winnewisser, A. Perrin, J.M. Flaud, J. Mol. Spectrosc. 195 (1999) 154.
[50] P.A. Giguere, T.K.K. Srinivasan, J. Raman, Spectrosc 2 (1974) 125.
[51] J.A. Boatz, M.S. Gordon, J. Phys. Chem. 93 (1989) 1819.
[52] G. Schaftenaar, J.H. Noordik, J. Comput.-Aided Mol. Design. 14 (2000) 123.
[53] Benjamin J. Lynch, Donald G. Truhlar, J. Phys. Chem. A. 105 (2001) 2936.
[54] Benjamin J. Lynch, Patton L. Fast, Maegan Harris, Donald G. Truhlar, J. Phys. Chem. A. 104 (2000).
[55] Y. Tarchouna, M. Bahri, N. Jaïdane, Z. Ben Lakdar, J. Mol. Struct.(-THEOCHEM) 758 (2006) 53.
[56] B.C. Garrett, Donald G. Truhlar, J. Phys. Chem. 83 (1979) 1915.